Finite element model updating of a semi-rigid moment resisting structure

Alireza T. Savadkoohi[1,*,†], Marco Molinari[1], Oreste S. Bursi[1,‡]
and Michael I. Friswell[2,§]

[1]*Department of Structural and Mechanical Engineering, University of Trento, via Mesiano 77, 38100, Trento, Italy*
[2]*School of Engineering, Swansea University, Swansea SA2 8PP, U.K.*

SUMMARY

Partial-strength composite steel–concrete moment-resisting frame structures can be designed to develop a ductile response in components of beam-to-column joints and column bases, including flexural yielding of beam end plates, shear yielding of column web panel zones and yielding of anchors. To evaluate the performance of a statically indeterminate structure under different earthquake intensities, a series of pseudo-dynamic, quasi-static cyclic and vibration tests were carried out at the European Laboratory for Structural Assessment of the Joint Research Centre at Ispra, Italy. The identified modal parameters from forced vibration tests at three different damage levels were used in order to quantify local and global damage indices by updating a 3D FE model of the structure with the non-linear Powell's Dog-Leg optimization method. Then, the Latin Hypercube Sampling technique, a variant of the Monte Carlo method, was employed to study the sensitivity of the updated parameters of the 3D model to modal inputs, caused by measurement noise. Rotations of beam-to-column joints and column bases, storey displacements and forces were employed during the final cyclic test in order to update a 2D FE model of the test structure. To avoid numerical instabilities during the detection of the non-linear behaviour of the structure, a novel technique based on the transformation of the origin coordinates in each half cycle was implemented. The identified joint behaviours allowed low-cycle fatigue energy-based damage indices to be applied. Copyright © 2009 John Wiley & Sons, Ltd.

1. INTRODUCTION

A seismic design option in modern steel and steel–concrete composite structures is represented by semi-rigid beam-to-column joints that are able to accommodate inelastic rotations through ductile inelastic component responses [1,2]. Thus, global beam hinging mechanisms for earthquake resistance can be achieved at a reduced cost as the force demand in joints and columns is governed by the expected capacity of the ductile connection components rather than by the beam flexural capacity. In this respect, detection and evaluation of the actual damage due to earthquakes in these structures becomes different to that in structures with rigid joints. The work described in this paper has been performed as part of two European projects [3,4] where a series of vibration experiments followed the application of pseudo-dynamic (PsD) and

---

*Correspondence to: Alireza T. Savadkoohi, Department of Structural and Mechanical Engineering, University of Trento, via Mesiano 77, 38100, Trento, Italy.
†E-mail: alireza.savadkoohi@ing.unitn.it
‡Professor of Structural Dynamics and Control.
§Professor of Aerospace Structures.

quasi-static cyclic loadings on a semi-continuous moment resisting (MR) structure. The specimen was constructed and tested at the European Laboratory for Structural Assessment (ELSA) of the Joint Research Centre (JRC) in Ispra, and consisted of a full-scale two-storey two-bay frame with concrete slab dimensions in plan of $12.8 \times 7.4\,\text{m}^2$, and $7.0\,\text{m}$ in height. The testing programme included a sequence of PsD tests, simulating earthquakes with peak ground acceleration (pga) scaled up to the collapse onset limit state (COLS), followed by a final cyclic test. The MR structure behaved well under seismic loading and details of the seismic design and performance can be found in [5,6].

Recently, the evaluation of damage owing to seismic loading was performed by means of damage detection techniques that rely on FE structural models and on the observation that structural frequencies decrease with damage while damping ratios increase. The initial FE model of a structure is often a poor representation of its characteristics because of unavoidable simplifying assumptions; for instance, modelling the actual behaviour of semi-rigid joints in a semi-continuous structure can be a challenging task. It is evident that experimental data provide valuable information of how the structure behaves with regard to the initial FE model. As a result, the FE model can be corrected in an updating procedure that belongs to the class of inverse problems in classical mechanics [7].

Model updating methods can be classified as sensitivity or direct methods [7]. Sensitivity-type methods rely on a parametric FE model of the structure and the minimization of some penalty functions based on the error between measured and predicted data. Direct updating methods are based on changes to complete mass and/or stiffness matrices and generally the updated models obtained are difficult to interpret. Model updating of structures can rely on different data types: (i) data from dynamic tests and (ii) data retrieved from static or quasi-static tests. Dynamic-based identification techniques are more mature and therefore the corresponding literature is quite extensive.

Doebling *et al.* [8] provided an overview of methods able to detect, locate and characterize damage in structural systems using the measured vibration response. Teughels *et al.* [9,10] used modal models as well as damage functions controlled by a limited number of parameters in order to estimate the bending stiffness distribution along beam-type structures. Bakir *et al.* [11] introduced an improved FE model updating scheme and a novel global optimization that was applied to a residential building subjected to the 1999 Kocaeli and Duzce earthquakes. Rahai *et al.* [12] presented an approach for damage detection by considering structures with simple or rigid joints utilizing incomplete measured mode shapes and natural frequencies. The effect of data polluted by noise was considered by means of Monte Carlo simulations. Amani *et al.* [13] identified damping and stiffness matrices both of a tested reinforced concrete beam and of a reduced scale six-storey aluminium plane frame structure subjected to ambient loading.

Applications of static-based identification techniques are rather limited, mainly because global quantities are not involved. Some attempts have also been made to identify structures under static loads. Sanayei and Saletnik [14,15] suggested a method for structural identification by using a subset of applied static forces and a subset of noisy measured strains. Liu and Chian [16] identified the element properties of a truss by the strains of truss elements measured during static tests. A damage identification algorithm using static test data and changes in natural frequencies was presented by Wang *et al.* [17]. In order to locate damage in the structure, the damage signature matching technique was improved through a proper definition of measured damage signatures and predicted damage signatures.

With regard to the damage evaluation of beam-to-column joints, Wong *et al.* [18], Koh *et al.* [19] and Wu and Li [20], among others, identified damage in joints of steel framed structures. These studies were successful in joint identification, although only simple beam-to-column joint models in the elastic range were considered. Moreover, they highlighted that the damage detection of semi-rigid joints experiencing severe inelastic damage, and more generally of composite structures characterized by low masses, low damping and complex geometry, remains largely unexplored. This paper investigates the subject in more depth.

Three separate vibration test series were performed on the MR steel–concrete composite test structure: first, on the intact, undamaged structure; second, after attaining the life safe limit state; and finally, after the structure had suffered severe cyclic loadings [4,21]. The structure was subjected to both sinusoidal and impulsive excitation and its response was recorded via three different

configurations of accelerometers: one arrangement for the overall or global structural response and two sets for the analysis of interior and exterior joints, respectively. Since the structure was in a laboratory, the damage imposed was known and the bare structure could always be inspected.

The main characteristics of the prototype test structure, test programme, instrumentation and main results of the modal extraction are summarized in Section 2. The non-linear Powell's Dog-Leg (DL) technique employed in the model updating is discussed in Section 3. The 3D FE model, of both the structure and the joints, are briefly described in Section 4, together with the modal updating technique based on the DL method and the corresponding results. Both local and global damage indices of the MR structure are computed in this section, based on measured and updated FE quantities [22]. The Latin Hypercube Sampling (LHS) technique [23], which is a variant of the Monte Carlo method, is described and used to analyse the sensitivity of the updated parameters to measurement errors. In Section 5, a 2D FE model of the structure is introduced and model updating under cyclic loads is proposed, with the identification of the hysteretic behaviour of damaged joints. Damage indices of the structural joints are also computed using low-cycle fatigue energy-based damage models [24]. Conclusions and perspectives are summarized in Section 6.

2. DESCRIPTION OF THE STRUCTURE AND TEST PROGRAMME

2.1. The test structure

The prototype two-storey structure shown in Figure 1(a) was selected to have representative dimensions, member sizes and connection details in order to study the seismic behaviour of steel–concrete composite structural systems. The structure includes five identical two-bay moment-resisting frames with unequal spans. The test structure was a two-storey, two-bay building specimen 7 m high with plan dimensions from centre to centre of two exterior columns equal to $6.0 \times 12.0\,m^2$; dimensions of the composite slabs were slightly greater. The model was constructed with three MR frames shown in Figure 1(b), with unequal spans of 5.0 and 7.0 m, respectively. Steel–concrete composite beams were formed by IPE300 steel profiles connected by full shear connection studs to a 15-cm-thick concrete slab, cast on profiled sheeting. HEB260 and HEB280 partially encased steel–concrete composite columns were used and high-ductile partial-strength composite beam-to-column joints were designed to provide plastic joint rotations of 35 mrad associated with a residual strength of at least 80% of their maximum value [2] under earthquake loading. In the transverse direction, secondary beams were pinned and connected to column webs; and as illustrated in Figure 1(c), two concentrically braced frames were designed to prevent any lateral instability. Each concrete slab was extended along the longitudinal and transverse directions of the exterior beam-to-column joints in order to provide additional resistance to hogging bending moments and to achieve the effective width of longitudinal composite beams. Figure 1(d) shows the general view of the test structure. Braconi *et al.* [5,6] provided more detailed information about the design and performance of the test structure.

2.2. Test programme

The performance of the benchmark structure was investigated at four different pga levels during the PsD tests. The test levels were as follows: 0.1 g in order to characterize the pseudo-elastic state; 0.25 g for the Serviceability Limit State (SLS); 1.4 g for the Life Safe Limit State (LSLS); and 1.8 g for the COLS. A final cyclic test beyond the COLS was also performed. Table I summarizes the test programme, with relevant objectives.

Three vibration tests were carried out at different damage phases to perform damage detection and quantification: Phase I for the identification of the intact structure; Phase II for the identification at the LSLS; Phase III for the identification beyond the COLS. Both in PsD and cyclic tests, four actuators were connected at one end of the structure.

In order to improve design methods and to enhance knowledge of the joint behaviour, preliminary monotonic and cyclic tests on beam-to-column and base joints were carried out at
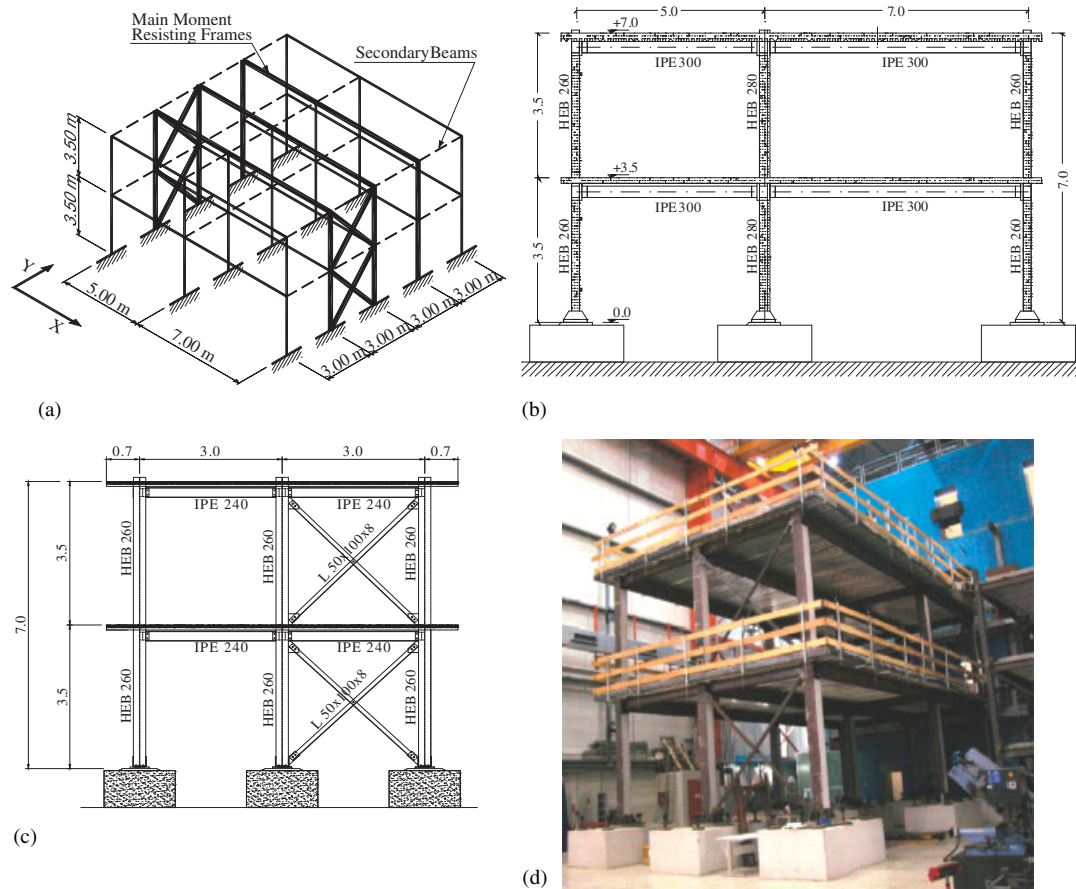
Figure 1. The test MR structure: (a) designed and tested structure; (b) side view; (c) end view; and (d) general view.

Table I. Summary of the test programme and performance objectives.

Test	Vibration test	PsD test-pga (g)	Performance objective
I	Phase I		Identification at the Undamaged State
1		0.10	Pseudo-elastic State
2		0.25	Serviceability Limit State
3		1.40	Life Safe Limit State (LSLS)
II	Phase II		Identification at the LSLS
4		1.80	Collapse Onset Limit State (COLS)
5		Cyclic	Maximum top displacement equal to 300 mm
III	Phase III		Identification beyond the COLS

the Universities of Pisa and Trento, Italy, respectively [25]. Test results were also exploited to estimate initial stiffness values for the modal updating procedure described in Section 4.3.

2.3. Dynamic tests, instrumentation and modal extraction

Forced vibration tests were carried out in the three Phases reported in Table I. These consisted of Stepped Sinusoidal Tests and Shock Hammer Tests, performed by means of an electro-dynamic shaker ELECTRO-SEIS 400 with 33.79 kg of total mobile mass and an instrumented sledge-hammer PCB 086D50 with a total mass of 10.77 kg, respectively. Figure 2 shows the locations of the excitation forces. Three different accelerometer configurations were employed in

each test [21]. To acquire accelerations corresponding to the six global degrees of freedom of the structure, i.e. four translational and two torsional modes, a total of six accelerometers were mounted on the structure as illustrated in Figure 2. In addition, local configurations, labelled B and C in Figures 3(a, c), were used to characterize the local dynamic behaviour of interior and exterior beam-to-column joints, respectively. This was achieved by accelerometers mounted
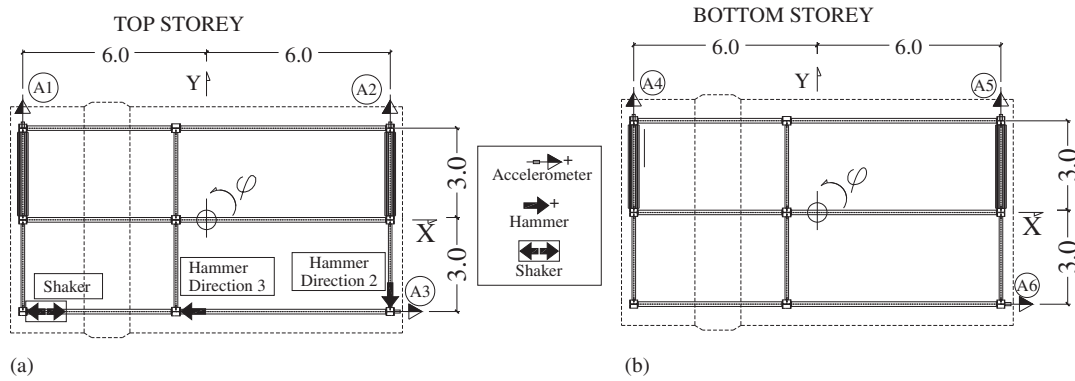

Figure 2. Location of the excitation devices and global configuration A of the accelerometers: (a) location of sensors in the top storey and (b) location of sensors in the bottom storey.
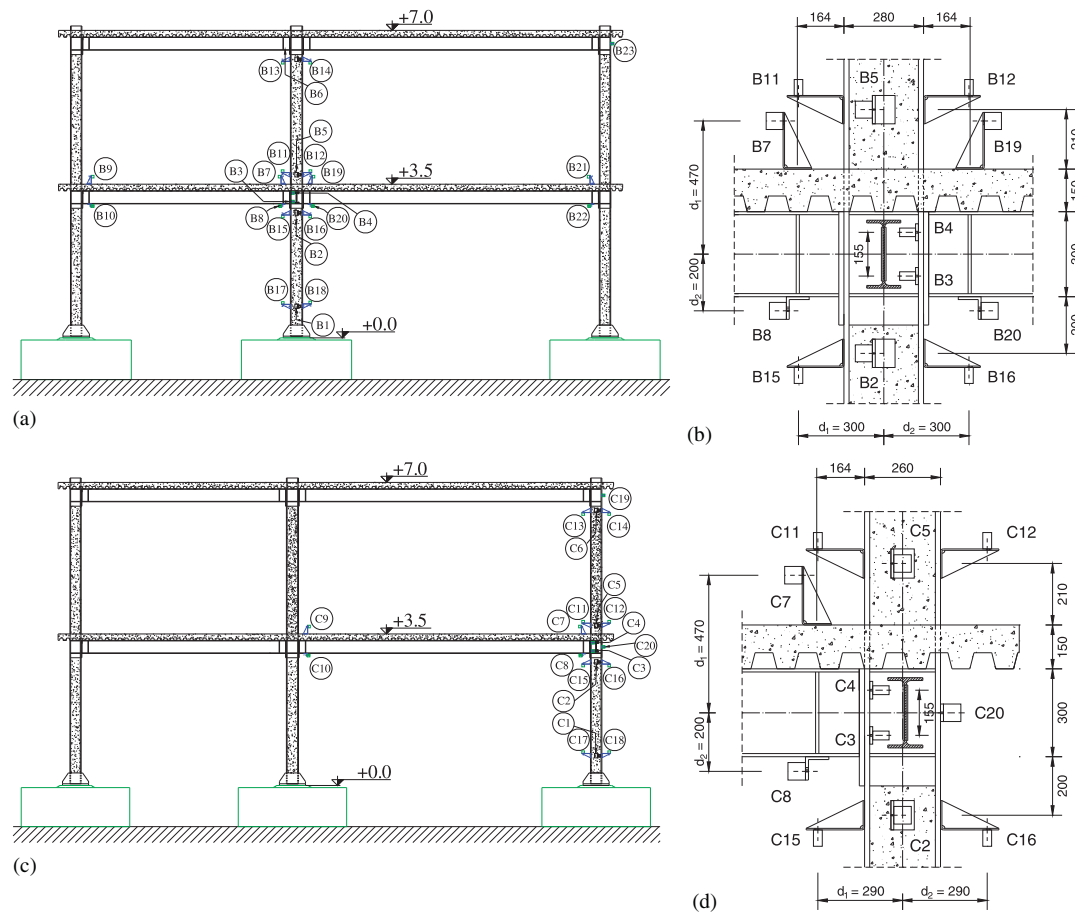

Figure 3. Local configurations of accelerometers: (a) interior members; (b) interior beam-to-column joints; (c) exterior members; and (d) exterior beam-to-column joints.

horizontally on the column flanges to acquire the web panel angular accelerations, shown in Figures 3(b, d), respectively. Translational and rotational accelerations were acquired on instrumented sections of both beams and columns, by arranging pairs of accelerometers above and below member axes. To improve the rotation measurements, accelerometers were well separated. With the same set-up, few kinematic components of some base joint rotations were also monitored, as shown in Figures 3(a, c).

The six lowest natural frequencies of the structure, corresponding to translational and torsional modes, were evaluated by the dynamic tests. Being well separated, eigenvalues, eigenvectors and viscous damping coefficients were extracted by the circle-fit modal analysis technique [26]. The resulting modal data are presented in Table II and the progressive reduction of the natural frequencies with damage, with an associated increase in the damping coefficients, is evident. Because of the fact that low energy dynamic tests were performed by means of the aforementioned exciters, the level of noise from the accelerometers may have introduced uncertainties in the damping ratios associated with higher modes. This trend can be noted in the torsional first mode, i.e. Mode 3 in Table II, and with the flexural and torsional second modes, i.e. Modes 4–6. The results are also in line with values identified by more complex identification techniques [27].

2.4. Cyclic test protocol and instrumentation

The sinusoidal displacement protocol shown in Figure 4, characterized by stepwise increasing amplitudes, was applied at the top storey through two actuators, whilst the actuators at the bottom storey were controlled to keep the bottom/top storey reaction force ratio equal to 0.97 for the whole test. That ratio was determined from examining the first mode shape of the structure after the COLS. The corresponding bottom storey displacement is illustrated in Figure 4 and is

Table II. Experimental natural frequencies and damping coefficients extracted from both SST and SHT tests.

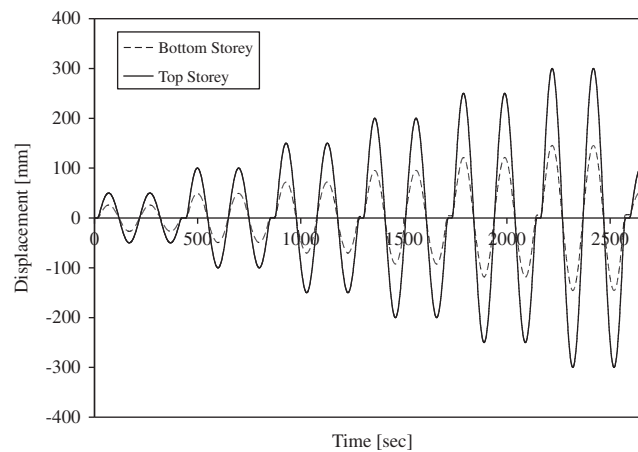| Mode	Phase I Frequency (Hz)	Phase I Damping (%)	Phase II Frequency (Hz)	Phase II Damping (%)	Phase III Frequency (Hz)	Phase III Damping (%)
1	3.36	0.57	2.38	1.27	1.95	1.44
2	5.09	0.66	4.44	0.83	4.15	0.96
3	6.92	0.70	6.24	0.67	5.70	0.68
4	10.94	0.69	8.95	0.61	8.18	0.90
5	16.48	0.49	13.95	0.30	13.72	0.59
6	22.52	0.76	19.97	0.54	19.05	0.44

Figure 4. Displacement protocols relevant to bottom and top storeys utilized during the cyclic testing.
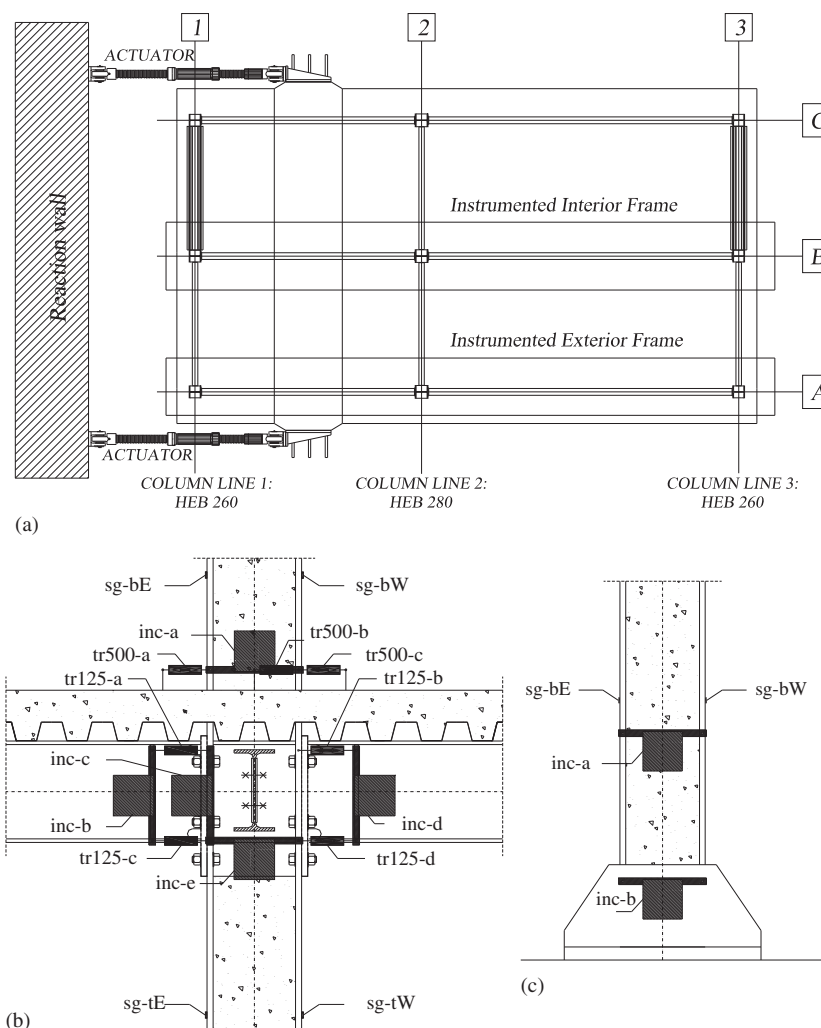
Figure 5. Test structure employed during cyclic testing: (a) instrumented frames; (b) interior joints (2-B) at the bottom storey; and (c) base joint (2-B).

also characterized by a displacement increment of 50 mm between cycles of increasing amplitude, with two equal cycles, up to a maximum of 300 mm at the top storey [4]. Two frames of the structure, shown in Figure 5(a), are referred to as the exterior (A) and interior (B) frames, and were instrumented by means of Strain Gauges (SG), Inclinometers (Inc) and Transducers (Tr). Typical sensor lay-outs of an interior joint as well as column base joints are illustrated in Figures 5(b, c), respectively. All measurements obtained from inclinometers and storey displacements and forces were used for cyclic model updating, described in Section 5.2.

3. POWELL'S DOG-LEG OPTIMIZATION TECHNIQUE

FE-based model updating procedures can be regarded as minimization processes in which the discrepancies between numerical and experimental data are minimized by adjusting unknown model parameters. The objective function, $F(\mathbf{p})$, is the L_2-norm of the errors between the vectors of analytical and experimental data, and is minimized by seeking optimal parameter values through an inverse modelling process. A local minimizer, $\mathbf{p}^*$, is searched in the least squares problem,

$$F(\mathbf{p}) = \tfrac{1}{2}\Delta(\mathbf{p})^{\mathrm{T}}\Delta(\mathbf{p}) \tag{1}$$

where $\Delta(\mathbf{p})$ is the given residual vector function.

Optimization algorithms are iterative in nature [28]. The process starts with an initial guess of the optimal values of the variables and proceeds by generating a sequence of improved estimates until a solution is reached. The strategy used to move from one iteration to the next distinguishes one algorithm from another. Two well-known methods are the Steepest Descent (SD) and the Trust Region (TR) methods. The SD method is a line search method in the opposite direction to the gradient of $F(\mathbf{p})$, i.e. $\mathbf{h}_{\text{SD}} = -\nabla F_t(\mathbf{p})$, at the t-th iteration, and where the step length is chosen in various ways. TR methods generate steps by utilizing a quadratic model of $F(\mathbf{p})$. They define a region around the current iterate within which they trust the model to be an adequate representation of $F(\mathbf{p})$. The step is then chosen to minimize this approximate model in the trust region, and the direction and length of the step are determined simultaneously. If a step is not acceptable, the size of the region is reduced and a new minimizer is found. In general, the step direction changes whenever the size of the trust region is altered.

Powell's Dog Leg (DL) method [28] belongs to the category of TR methods, but is a hybrid technique based on a combination of the Gauss–Newton (GN) and SD methods. A major problem with the DL method is the mechanism used to switch between the two methods when it is appropriate. Depending on the solution at the previous step, the DL method builds a trust region where the radius changes automatically depending on whether the step is far or close to a minimum. Let $\mathbf{p}_t$ and $\mathbf{h}_t$ be the current estimate of the parameter vector and the parameter increment at the t-th iteration, respectively. Then there are two candidates for the step to be taken from the current position $\mathbf{p}_t$, given by steepest descent, $\alpha\mathbf{h}_{\text{SD}}$ (where α is determined by a line search), and GN, $\mathbf{h}_{\text{GN}}$. The strategy to choose the DL step size ensures that $\|\mathbf{h}_{\text{DL}}\| \leqslant R$, where R is the radius of the TR. This radius is adjusted at each iteration depending on the quality of the second order Taylor series approximating the penalty function. Madsen *et al.* [28] gives further details.

There are two main stopping criteria for the algorithm:

(a)   the gradient $\nabla F(\mathbf{p})$ approaches zero, or

$$\|\nabla F(\mathbf{p})\|_{\infty} \leqslant \varepsilon_1 \tag{2}$$

where $\|\nabla F(\mathbf{p})\|_{\infty}$ is the infinite norm of $\nabla F(\mathbf{p})$ and ε_1 is a very small positive number,

(b)   the change in the parameters is small, or

$$\|\mathbf{p}_{t+1} - \mathbf{p}_t\| \leqslant \varepsilon_2(\varepsilon_2 + \|\mathbf{p}_t\|) \tag{3}$$

where ε_2 is also a very small positive number. This stopping criterion modulates the relative step size from ε_2 when $\|\mathbf{p}_t\|$ is large to ε_2^2 when $\|\mathbf{p}_t\|$ is close to zero.

4. IDENTIFICATION AND DAMAGE EVALUATION UNDER DYNAMIC LOADING

4.1. The 3D FE model of the structure under dynamic load

Model updating was performed using a 3D FE model of the benchmark structure with 429 degrees of freedom, shown in Figure 6(a), which was assembled and implemented in Mathematica [29]. The model had three identical frames (see Figure 6(b)) that were connected through master–slave numerical constraints at each storey level. The constraints were the horizontal displacements within each storey and the rotations about the vertical axis. Beam-to-column elements were used to simulate the behaviour of members, while braces were modelled by means of truss elements. Shear panels were modelled by means of four pinned rigid bars that were stabilized by a rotational spring. The behaviour of the beam-to-column connections were simulated by rotational springs jointing the beams to the shear panels. Details of the structural joints are summarized in Figure 6(c). The simplified joint model of Figure 6(d) was conceived and implemented to limit the number of degrees of freedom. A lumped mass model was used, where the mass distribution was assumed to be known. The bottom storey had a mass of 43 171 kg and the top storey a mass of 39 332 kg. The masses and moments of inertia of the storeys were applied directly to the master degrees of freedom. A linear
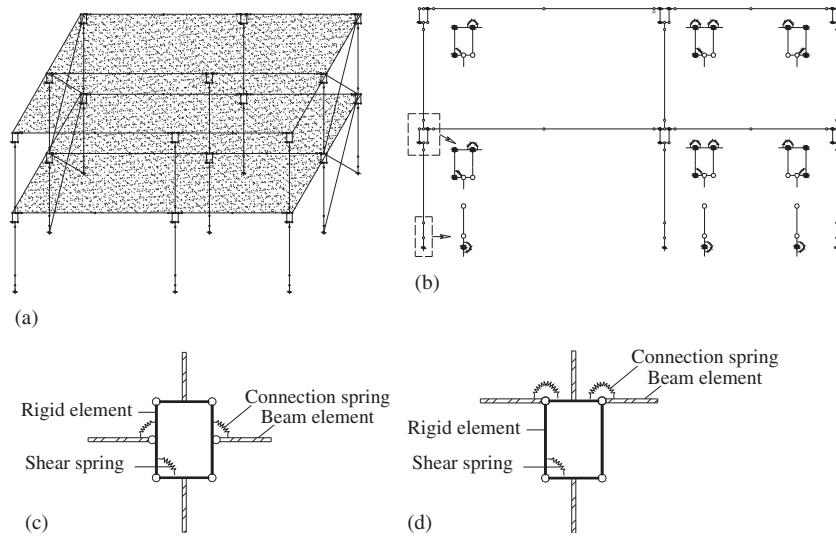
Figure 6. FE model of the benchmark structure: (a) 3D model; (b) 2D model of the interior frame; (c) beam-to-column joint model; (d) simplified beam-to-column joint model.

elastic behaviour for all structural elements was assumed owing to the updating strategy presented here.

4.2. The sensitivity approach for model updating

A sensitivity-based approach was chosen for model updating [7]. The approach minimizes $F(\mathbf{p})$ based on the difference between the measured and predicted modal quantities. The variations between the r-th eigenvalues and eigenvectors, $\Delta\lambda_r$ and $\Delta\varphi_r$, are obtained from the experimental results, $[\lambda_{Xr}, \varphi_{Xr}^{\mathrm{T}}]^{\mathrm{T}}$, and the computed results at parameter vector $\mathbf{p}$, $[\lambda_{Ar}, \varphi_{Ar}^{\mathrm{T}}]^{\mathrm{T}}$. The eigenvalue residuals are weighed [30] so that

$$\boldsymbol{\Delta}_t(\mathbf{p}) = \begin{pmatrix} \dfrac{\Delta\lambda_1}{\lambda_{A1}} \\ \Delta\varphi_1 \\ \vdots \\ \dfrac{\Delta\lambda_m}{\lambda_{Am}} \\ \Delta\varphi_m \end{pmatrix} \tag{4}$$

The residuals are then written as a Taylor series expansion,

$$\boldsymbol{\Delta}_t = -\mathbf{J}_t\mathbf{h}_t \quad \text{where } \mathbf{h}_t = \begin{pmatrix} h_{t1} \\ \vdots \\ h_{tN_{\mathrm{p}}} \end{pmatrix}, \tag{5}$$

h_{tj} is the j-th element of the parameter perturbation vector $\mathbf{h}_t$ at the t-th iteration and N_{p} is the number of parameters. The matrix $\mathbf{J}_t$ in Equation (5) contains the eigenvalue and eigenvector derivatives with respect to the parameters. These derivatives are called sensitivities and are calculated using the methods suggested in [31,32]. Usually eigenvalue sensitivities are one order of magnitude greater than the mass-normalized eigenvector sensitivities [30].

The standard Newton–Raphson method was not able to minimize $F(\mathbf{p})$ satisfactorily, because $\mathbf{J}_t$ was rectangular, affected by noise and hence ill-conditioned. Thus, Powell's Dog-Leg

method, described in Section 3, was used. For this particular case, the initial radius for TR method was $R_0 = 1$, while $\varepsilon_1 = \varepsilon_2 = 10^{-4}$ in Equations (2) and (3).

The lack of correlation between the experimental and predicted quantities may result from modelling simplifications that generate many spurious numerical modes, and modal shifts may be experienced during iterations. The Modal Assurance Criterion (MAC) [26] was used systematically as a measure of the modal correlation, and this produces a matrix of inner products between the mode shape vectors. Only the first five experimental modes listed in Table II correlated well with the model and were therefore retained for model updating. Furthermore, only a few modal rotational components of the beams were used, since the lower modes involve only limited joint rotation and accuracy of measurements was therefore reduced.

4.3. Updating parameters and damage indices

Because of the ill-conditioned nature of $\mathbf{J}_t$ in Equation (5), the number of parameters (N_p) for complex members and joints must be limited. Thus, the major issue is how to parameterize the unknown quantities in a convenient way, taking into account the limited experimental information and the limited influence of some parameters on the five experimental modes considered. A preliminary analysis of the FE model shown in Figure 6(a) highlighted that the model was:

(i) not sensitive to the bending and torsional stiffness of beams and the rotational stiffness of shear panels;
(ii) sensitive to bending stiffnesses of columns in the longitudinal direction;
(iii) sensitive to the axial stiffness of braces in the transverse direction;
(iv) sensitive to the rotational stiffness of beam-to-column connections and the rotational stiffness of base joints in the longitudinal direction.

This information was supplemented by analysing the rank or non-zero singular values of the sensitivity matrix $\mathbf{J}_t$; the number of updating parameters, $\mathbf{p}_t$, cannot exceed the rank of $\mathbf{J}_t$. Primarily, the FE model was updated by using only seven parameters related to the stiffness of the structural elements given above. Calculating the singular values of the sensitivity matrix in this case shows that only three singular values are significant. As a result, only the following three parameters were retained and estimated. Thus, in a general form,

$$K = p_j K_0 \quad \text{for } j = 1, 2, 3 \tag{6}$$

where K_0 defines the baseline stiffness corresponding to each parameter. The three parameters correspond to the element groups (ii), (iii) and (iv) listed above. The initial values for each parameter in Equation (6) for Phase I were available from preliminary beam-to-column and column base joint cyclic tests [25]. Cyclic test data were also used as initial values for the identification process in Phase III. Initial values for each parameter group and Phase are listed in Table III. Updated stiffness values show a general reduction of stiffness from Phase I to Phase III. As expected, stiffness reductions are more evident for beam-to-column and column base joints, where energy dissipation was sought by proper seismic design [5,6].

The paired natural frequencies obtained by model updating and the relative errors with respect to the experimental frequencies are reported in Table IV. Larger errors are associated with frequencies of Phase II, which did not benefit from additional experimental information as for the other phases. Relatively large errors in the higher modes were expected, as these modes are more sensitive to modelling errors. Diagonal MAC indices are also reported in Table IV and a favourable correlation between updated and experimental mode shapes is evident.

Local damage indices that define a degradation measure at the structural level were computed for each phase. The local damage indices are defined as $D_L = 1 - k_{\text{Updated}}/k_{\text{Undamaged}}$, where $k_{\text{Undamaged}}$ and k_{Updated} indicate stiffnesses of virgin and damaged states, respectively [33]. Damage values indicating stiffness variations from Phase I to Phase II, i.e. $D_{L,I-II}$ and from Phase I to Phase III, i.e. $D_{L,I-III}$, are listed in Table V. $D_{L,I-II}$ values indicate that there is

Table III. Initial and updated element stiffnesses in the three test Phases.

Parameter	Element	Phase I		Phase II		Phase III	
		Initial	Updated	Initial	Updated	Initial	Updated
p_1	$EI_{Long., HEB260}$ (N m^2)	3.81E7	3.80E7	3.81E7	3.76E7	3.81E7	3.68E7
	$EI_{Trans., HEB260}$ (N m^2)	2.11E7	2.10E7	2.11E7	2.04E7	2.11E7	1.92E7
	$GJ_{t,HEB260}$ (N m^2)	1.47E7	1.45E7	1.47E7	1.43E7	1.47E7	1.37E7
	$EI_{Long., HEB280}$ (N m^2)	4.99E7	4.98E7	4.99E7	4.93E7	4.99E7	4.81E7
	$EI_{Trans., HEB280}$ (N m^2)	2.7E7	2.77E7	2.7E7	2.69E7	2.7E7	2.53E7
	$GJ_{t,HEB280}$ (N m^2)	1.97E7	1.95E7	1.97E7	1.91E7	1.97E7	1.84E7
p_2	EA_{braces} (N)	5.24E8	2.78E8	5.24E8	2.48E8	5.24E8	1.93E8
p_3	$K_{\phi,int.con.}$ (N m/mrad)	1.0308	1.02E8	4.23E7	4.17E7	1.61E7	3.19E7
	$K_{\phi,ext.con.}$ (N m/mrad)	1.08E8	9.71E7	3.83E7	3.30E7	6.24E6	1.24E7
	$K_{\phi,Long.,b.j.}$ (N m/mrad)	2.20E8	2.07E8	2.12E7	1.89E7	6.86E6	1.36E7
	$K_{\phi,Trans.,b.j.}$ (N m/mrad)	1.47E8	1.39E8	1.42E7	1.27E7	4.60E6	9.12E6

EI_{Long} is the flexural stiffness in the longitudinal direction; EI_{Trans} is the flexural stiffness in the transversal direction; GJ_t is the torsional stiffness; EA is the axial stiffness; $K_{\phi,int.con.}$ and $K_{\phi,ext.con.}$ are the rotational stiffnesses of beam-to-column connections of interior and exterior joints, respectively; $K_{\phi,Long.b.j.}$ and $K_{\phi,Trans.b.j}$ are the rotational stiffnesses of base joints in the longitudinal and transversal directions, respectively.

Table IV. Identified natural frequencies, percentage errors with respect to the experimental values of Table II, and the diagonal MAC indices between identified and experimental mode shapes.

	Phase I			Phase II			Phase III		
Mode	Frequency (Hz)	Error (%)	MAC	Frequency (Hz)	Error (%)	MAC	Frequency (Hz)	Error (%)	MAC
1	3.36	0.1	1.00	2.33	2.2	0.99	1.96	−0.4	0.95
2	5.04	1.0	1.00	4.63	−4.2	1.00	4.20	−1.1	1.00
3	7.02	−1.5	0.78	6.44	−3.2	0.84	5.80	−1.7	0.81
4	11.51	−5.9	0.96	9.69	−8.2	0.98	8.45	−3.4	0.83
5	15.45	6.3	0.82	12.85	7.9	0.87	11.91	16.0	0.79

Table V. Local damage indices D_L of structural members and joints.

Element	$D_{L,I-II}$	$D_{L,I-III}$
$EI_{Long., HEB260}$ (N m^2)	0.011	0.032
$EI_{Trans., HEB260}$ (N m^2)	0.029	0.086
$GJ_{t, HEB260}$ (N m^2)	0.014	0.055
$EI_{Long., HEB280}$ (N m^2)	0.010	0.034
$EI_{Trans, HEB280}$ (N m^2)	0.029	0.087
$GJ_{t, HEB280}$ (N m^2)	0.021	0.056
EA_{braces} (N)	0.110	0.310
$K_{\phi,int. con.}$ (N m/mrad)	0.590	0.690
$K_{\phi,ext. con.}$ (N m/mrad)	0.660	0.870
$K_{\phi,Long., b.j.}$ (N m/mrad)	0.910	0.930
$K_{\phi,Trans., b.j.}$ (N m/mrad)	0.910	0.930

practically no damage for columns, minor damage for braces and severe damage for beam-to-column connections and column base joints. After the PsD test at 1.4 pga (Table I), visual inspection showed that the braces lost stiffness due to light cracking of concrete at their ends. Concrete crushing happened in the composite slab close to the beam-to-column joints. Localized spalling of the grouting mortar from the bottom flange of base joints occurred because the anchoring rebars yielded [4]. After the final cyclic test (Table I), the structure was subjected to inter-storey drift ratios of about 4.6% at the second storey. This implied that the

beam-to-column joints at the bottom storey, see Figures 3(a, c), were also severely damaged with cracks in the end plates and column flanges. Again, damage values given in Table V qualitatively mirror these phenomena.

The global damage measure D_G of the structure in the phases considered above was estimated by a method based on the maximum eigenvalue of the flexibility matrix, $\mathbf{G}$, recovered from the structural eigenfrequencies and mode shapes obtained in Section 2. This method assures that the degradation process of the structure proceeds until the stiffness matrix becomes singular at failure, when the lowest eigenvalue of the tangent stiffness matrix approaches zero while the largest eigenvalue of the flexibility matrix tends to infinity [22]; moreover, it can avoid the costly procedure of model updating. The flexibility matrix, $\mathbf{G}$, can be computed more reliably than its inverse, $\mathbf{G}^{-1}$. This is because the lowest frequencies and corresponding mode shapes, measured from vibration tests, provide the largest contribution to $\mathbf{G}$. Conversely, the stiffness matrix $\mathbf{G}^{-1}$ is dominated by the highest modes that are rarely available from tests. Thus, the flexibility matrix is given by

$$\mathbf{G} = \varphi \mathbf{\Lambda}^{-1} \varphi^{\mathrm{T}} \tag{7}$$

where $\mathbf{\Lambda}$ is the matrix of experimental eigenvalues and φ the matrix of experimental eigenvectors. The largest eigenvalue of $\mathbf{G}$, ψ_{max}^{-1}, can be computed by solving the corresponding eigenvalue problem. Then D_G can be defined as:

$$D_G = 1 - \frac{\psi_{\mathrm{max,Undamaged}}^{-1}}{\psi_{\mathrm{max,Updated}}^{-1}} \tag{8}$$

The values of D_G obtained from $\mathbf{G}$ using the first three modes, and also by using six modes in Table II, are reported in Table VI. The values are almost identical, and hence show the limited effect of the modal truncation. Since $D_G \geqslant 0.4$ [33], this implies the structure was severely damaged after Phase II and III as validated by visual inspection [4]. The updated FE model can provide a more realistic flexibility matrix than those assembled using experimental data. The corresponding indices D_G are reported in Table VI and reflect a higher level of damage. Additional details can be found in [34].

4.4. Sensitivity analysis

In this subsection the updating procedure is tested in the presence of noise and a sensitivity analysis was performed to assess how robust the results are to measurements contaminated with noise. Standard Monte Carlo simulations were employed to investigate the properties of the estimation procedure. In order to reduce the number of simulations, the LHS technique (a stratified sampling technique that can be applied to multiple variable problems [23,35]) was used to generate more uniform samples with equal probability. In order to perform Monte Carlo-based simulations, random data between 0 and 1 have to be generated. The desired input variable can then be obtained with an appropriate inverse transformation of data.

Suppose we wish to select n different values from each of the m variables $X_1, X_2, \ldots, X_m$ by means of the LHS technique. The range of each variable is divided into n non-overlapping, equal probability intervals and one value from each interval is randomly sampled. The n values thus obtained for X_1 are paired in a random manner with the n values of X_2 and so on, until an $n \times m$ table is formed. This $n \times m$ table is the same as the $n \times m$ dimensional input vectors. However, this kind of ordering variables creates an inevitable correlation between the generated

Table VI. Global damage indices D_G of the structure.

Method	$D_{G,\text{I–II}}$	$D_{G,\text{I–III}}$
Based on three experimental Modes	0.4652	0.6274
Based on six experimental Modes	0.4650	0.6274
Based on the updated flexibility matrix	0.5212	0.6669

data. In order to impose the desired correlation matrix between m sets of generated variable data, the restricted pairing algorithm of Iman and Conover [36] was implemented. Thus, a synthetic data set able to reproduce a given correlation structure of actual data and to preserve the relevant marginal distribution was generated.

For the sake of simplicity, both the system and measurement noise of the test structure were directly simulated through variation in modal quantities. The Normal probability distribution was simulated, with mean values corresponding to experimental measurements and standard deviations σ as follows:

(a) eigenvalues:

$$\sigma_\lambda = 0.0004\lambda \qquad (9)$$

(b) displacement components of eigenvectors:

$$\sigma_{\phi_{d,i}} = 0.04 \times |\varphi_{d,\max}| + 0.04 \times |\varphi_{d,i}| \qquad (10)$$

(c) rotational components of eigenvectors:

$$\sigma_{\phi_{r,i}} = 0.075 \times |\varphi_{r,\max}| + 0.075 \times |\varphi_{r,i}| \qquad (11)$$

where λ, $\varphi_{d,i}$, $\varphi_{r,i}$, $\varphi_{d,\max}$ and $\varphi_{r,\max}$ are eigenvalues, modal displacements and rotations and relevant maximum values, respectively.

Because of the unknown correlation of the actual measurements, the analysis was repeated for two limiting cases by using both perfectly uncorrelated reference data and fully correlated reference data, respectively; the actual data being within these limits. The correlation matrix for the generated eigenvalue data in Phase I for fully correlated data is

$$\begin{bmatrix} 0.999 & 0.997 & 0.998 & 0.998 & 0.998 \\ 0.997 & 0.999 & 0.997 & 0.997 & 0.998 \\ 0.998 & 0.997 & 0.999 & 0.999 & 0.998 \\ 0.998 & 0.997 & 0.999 & 1.000 & 0.998 \\ 0.998 & 0.998 & 0.998 & 0.998 & 0.999 \end{bmatrix}, \qquad (12)$$

and for the fully uncorrelated data is

$$\begin{bmatrix} 0.999 & -0.021 & -0.071 & 0.066 & -0.019 \\ -0.021 & 1.000 & 0.065 & 0.069 & 0.000 \\ -0.071 & 0.065 & 1.000 & 0.030 & 0.084 \\ 0.066 & 0.069 & 0.030 & 0.999 & -0.001 \\ -0.019 & 0.000 & 0.084 & -0.001 & 0.999 \end{bmatrix}, \qquad (13)$$

thus showing the quality of the generated data. More details can be found in [37]. Table VII shows the coefficient of variation C_v of each updated parameter p_i. The kernel density $\hat{f}(p)$ plot of the updated parameters provided by the S-Plus software [38] relevant to braces and connection springs for each Phase are shown in Figures 7(a, c) for the uncorrelated input case, and in Figures 7(b, d) for the fully correlated input case, respectively. Results clearly show that the updated brace stiffness has the smallest variation, compared to stiffnesses of the columns and joints in all damage phases. This implies that the braces were modelled well, that the MR structure was very sensitive to the brace stiffness in the transverse direction and, hence, the braces were relatively insensitive to errors.

The behaviour of the structure in the longitudinal direction was mainly controlled by the column flexural stiffness and by beam-to-column and base joint rotational stiffnesses. The corresponding parameters appear to be more sensitive to noise and more difficult to identify with the sensor location highlighted in Figure 3 and the FE model shown in Figure 6, because

Table VII. Coefficient of variation C_v of updated members and joints.

Phase	Data	C_v		
		Columns	Braces	Connections and base joints
I	Uncorrelated	0.386	0.054	0.309
	Correlated	0.216	0.018	0.246
II	Uncorrelated	0.169	0.022	0.181
	Correlated	0.186	0.025	0.191
III	Uncorrelated	0.125	0.039	0.057
	Correlated	0.184	0.039	0.046
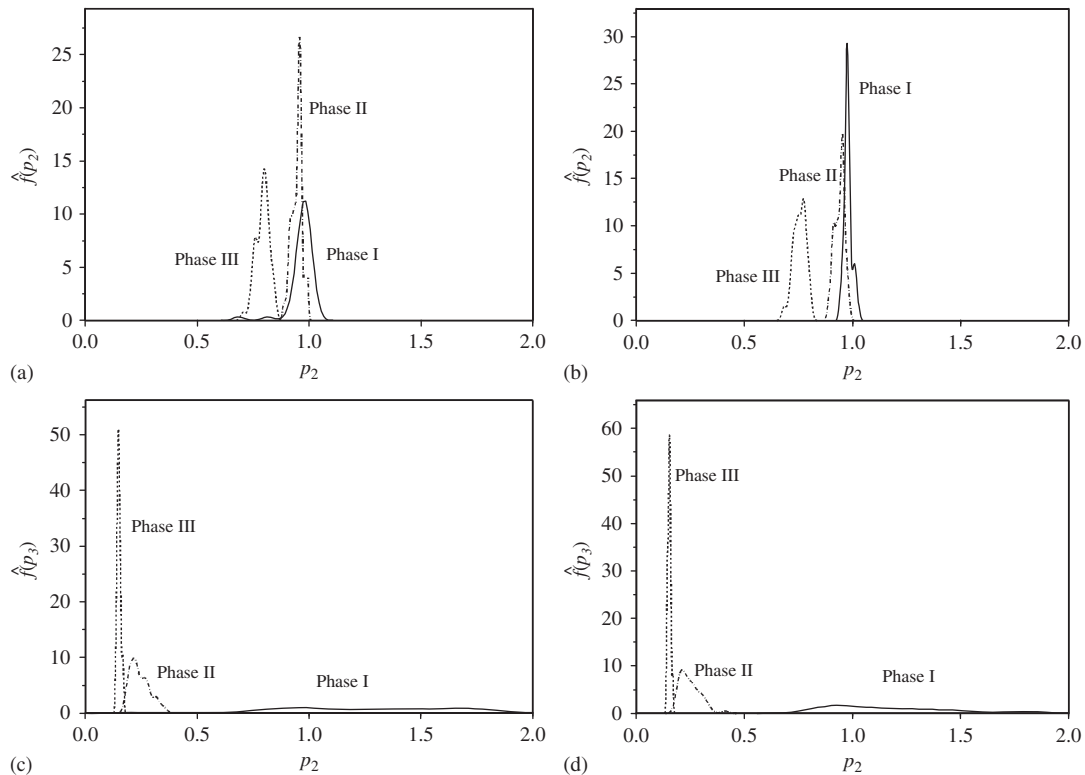
Figure 7. Kernel density $\hat{f}(p)$ plot [38] for the updated parameters of: (a) braces with uncorrelated input data: (b) braces with correlated input data; (c) connections and column base joints with uncorrelated input data; and (d) connections and base joints with correlated input data.

only two modes were significant in this direction. Furthermore, the sensitivity analysis shows that Phase I was the most sensitive Phase to noise, mainly because the structure was elastic and undamaged. Conversely, the parameter variations in Phases II and III became smaller for columns, connections and base joint stiffnesses, for two reasons: the exploitation of reliable initial stiffnesses that were obtained from model updating for the cyclic loading and the greater flexibility of the structure owing to the damage caused by severe cyclic loading.

5. IDENTIFICATION AND DAMAGE EVALUATION UNDER CYCLIC LOADING

5.1. 2D FE model of the structure

A 2D FE model of the interior frame with 168 degrees of freedom was employed to update the structure under cyclic loading. This model was considered appropriate because: (i) the three

main MR frames were the same (see Subsection 2.1); (ii) cyclic tests were performed only in one direction; (iii) the level of the static excitation was very severe; (iv) several sensors were employed (see Subsection 2.4). Therefore, beams and columns were modelled by means of the beam element formulation provided by the IDARC 2D software [39]. Figure 6(c) shows how the beam-to-column joints were modelled and the column base joints were modelled with springs and rigid links. The model was implemented in Mathematica [29] and the 2D FE model of the frame with joint numberings is shown in Figure 8.

5.2. Model updating methodology under cyclic loading

Thirty-two measurements were acquired from the instrumentation during the cyclic test in the form of time series, including rotations of joint components, external forces and storey displacements. The model updating of the structure under cyclic loading was based on the minimization of $F(\mathbf{p})$ defined in Equation (1), where $\boldsymbol{\Delta}(\mathbf{p})$ contains the residuals of the experimental and analytical aforementioned quantities. Twenty-five parameters were used to define the mechanical properties of different elements of the FE model in Equation (6). These parameters were: (i) three parameters for the rotational stiffness of each base joints; (ii) six parameters for the rotational stiffness of each shear panel; (iii) eight parameters for the rotational stiffness of each connection; (iv) four parameters for the flexural rigidity of each beam, long and short span at the top and bottom storeys; (v) four parameters for the flexural rigidity of columns, one parameter to the flexural rigidity of both lateral columns and one parameter to the middle column, at each storey. As a result, $\boldsymbol{\Delta}_t(\mathbf{p})$ at each iteration t was

$$\boldsymbol{\Delta}_t(\mathbf{p}) = \mathbf{U}_{Xt} - \mathbf{U}_{At} \tag{14}$$

where $\mathbf{U}_{Xt}$ and $\mathbf{U}_{At}$ are the experimental and analytical vectors, respectively, of rotations and displacements. The secant stiffness approach was employed to estimate rotations and displacements. Thus, following [37], Equation (14) can be expressed as

$$\boldsymbol{\Delta}_t(\mathbf{p}) = \mathbf{U}_{Xt} - \mathbf{K}_t^{-1}(\mathbf{p})\mathbf{L}_t \tag{15}$$

where $\mathbf{K}_t$ and $\mathbf{L}_t$ are the secant stiffness matrix and the external force vector imposed by the actuators, respectively. The corresponding Jacobian, $\mathbf{J}_t$, is

$$\mathbf{J}_t(\mathbf{p}) = -\frac{\partial(\mathbf{K}_t^{-1}(\mathbf{p})\mathbf{L}_t)}{\partial \mathbf{p}} = \mathbf{K}_t^{-1}(\mathbf{p})\frac{\partial \mathbf{K}_t(\mathbf{p})}{\partial \mathbf{p}}\mathbf{K}_t^{-1}(\mathbf{p})\mathbf{L}_t \tag{16}$$

Powell's Dog-Leg optimization method was implemented using an initial radius $R_0 = 1$ and $\varepsilon_1 = \varepsilon_2 = 10^{-6}$ in Equations (2) and (3).

In order to bypass numerical instabilities owed to the non-linear behaviour of the structure, especially when the secant stiffness becomes singular, as shown in Figure 9(a) for a single parameter, a novel method was conceived. The technique is based on the transformation of origin coordinates of all time series at each half cycle to their absolute maximum value and updating the structure half cycle by half cycle, as shown in Figure 9(b) [37]. Thus, after updating the FE model in the very first half cycle, all of the measured data were transformed to their own
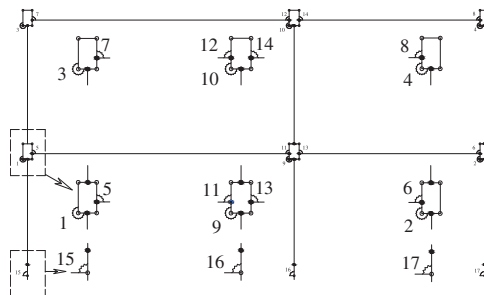

Figure 8. 2D FE model of the interior frame for model updating under cyclic loading.

absolute maximum values in all of the other half cycles. Hence, the FE was updated in each virtual half cycle, and then the identified results were transformed to their original values using the identified data from the previous half cycle. The implemented technique is fast as there is no need to implement complex algorithms to detect loading/unloading conditions.

The comparison between identified and experimental force–displacement relationships of the bottom and top storeys are highlighted in Figures 10(a, b), respectively. A good agreement between experimental and identified results is evident. As a result, the hysteretic behaviour of joint components of a statically indeterminate structure can be identified by cyclic model updating. Some of these relationships are shown in Figure 11, using the numbering of Figure 8. One can observe that the joint components exhibited a complex seismic performance complying with the requirements of Eurocode 8 for high ductility class MR frames [2].

5.3. Damage evaluation under cyclic loading

Structural damage of joints can be evaluated by information derived from the updated FE model. The low-cycle fatigue energy-based model proposed by Chai *et al.* [24] was employed to characterize structural damage. This model uses a damage index, D_i, based on both displacement and energy, and given by

$$D_i = \frac{\Delta_m}{\Delta_{um}} + \frac{\beta^*(E_h - E_{hm})}{V_y \Delta_{um}} \qquad (17)$$

where Δ_m is the maximum response displacement; Δ_{um} is the maximum displacement under a monotonic loading; E_h is the plastic strain energy dissipated by the components; E_{hm} is the plastic strain energy that is dissipated by the components under a monotonic loading. V_y is the yield strength of the component and β^* is a strength deterioration parameter that characterizes
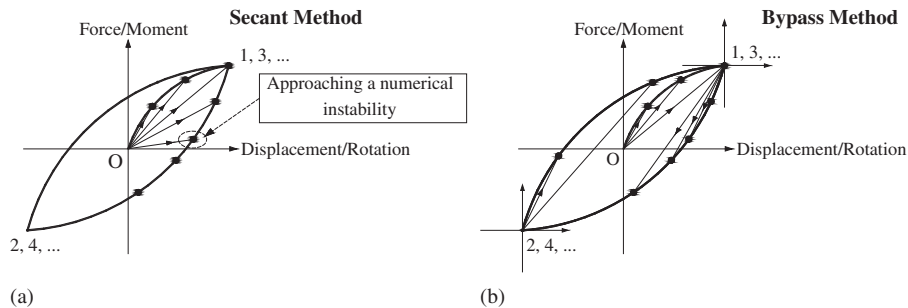

Figure 9. Model updating procedure under cyclic loading for a single parameter: (a) typical case involving numerical instabilities and (b) the transformation of origin coordinates in the bypass method.
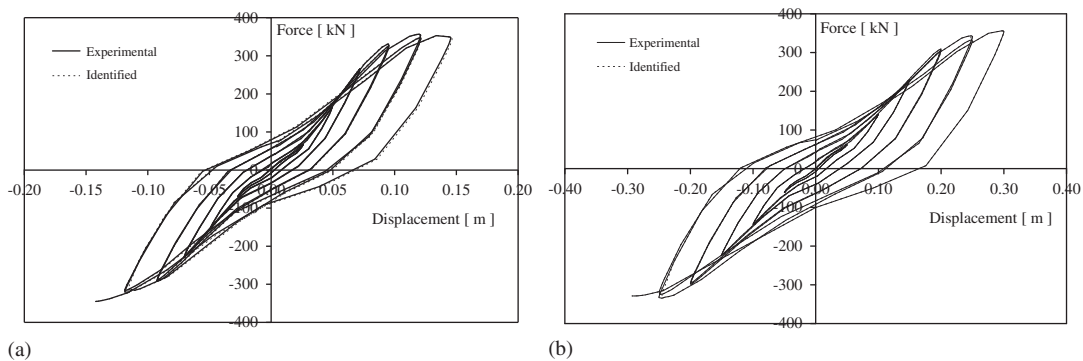

Figure 10. Comparison of updated and experimental force vs displacement: (a) bottom storey and (b) top storey.
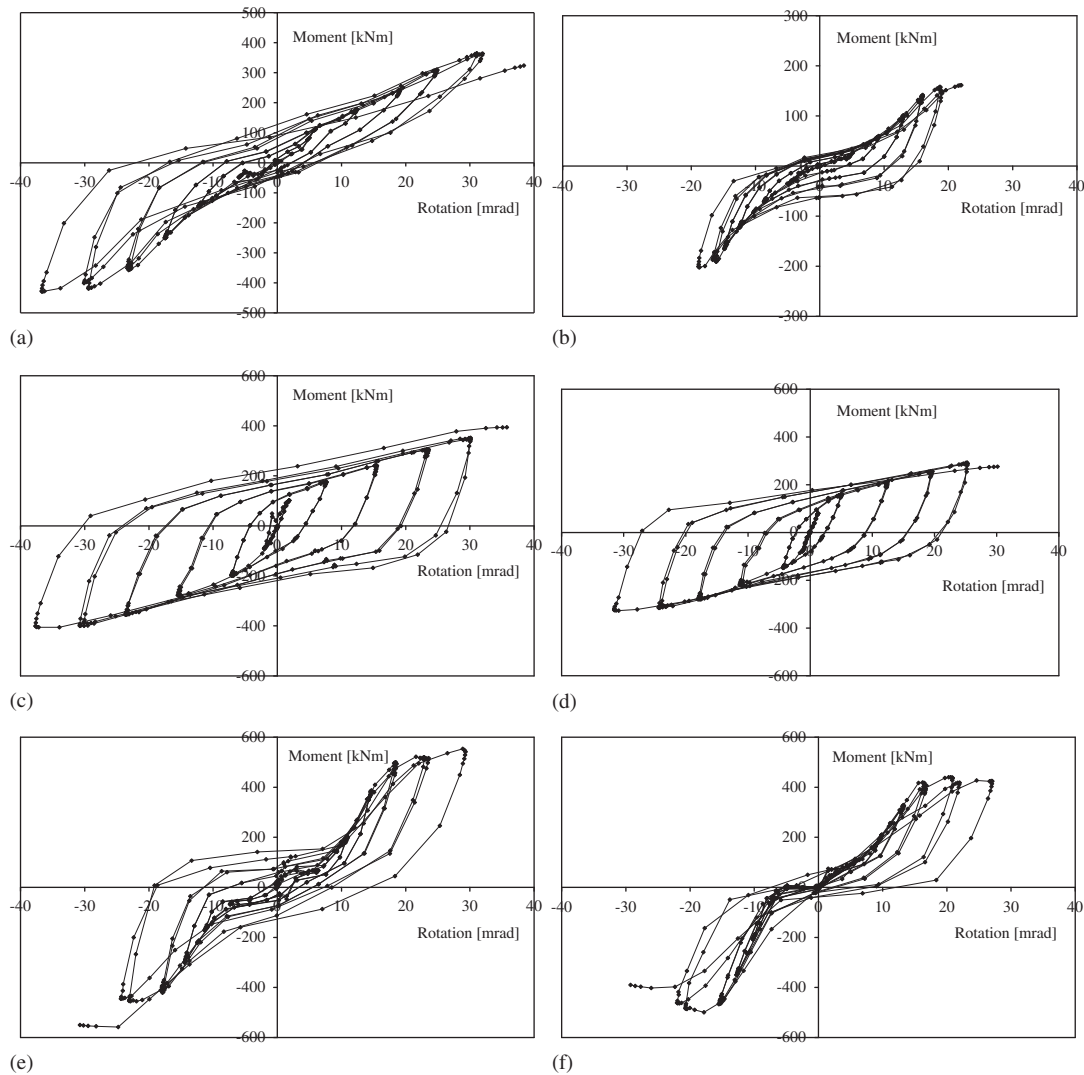
Figure 11. Identified joint components under cyclic loading: (a) connection, spring N.5; (b) connection spring N.8; (c) shear panel spring N.9; (d) shear panel spring N.10; (e) column base joint spring N.16; and (f) column base joint spring N.17.

the damage contribution owing to cumulative plastic strain energy. Typical damage index values D_i represent:

$$D_i < 0.4 : \text{minor damage.}$$

$$0.4 \leqslant D_i < 1 : \text{irreparable damage.}$$

$$D_i \geqslant 1 : \text{component collapse}$$

The parameter β^* can be obtained by calibrating the model against experimental data assuming that $D_i = 1$ corresponds to component collapse. As a result, from Equation (17), one gets:

$$\frac{E_h}{V_y \Delta_{um}} = \frac{1}{\beta^*} - \frac{1}{\beta^*} \frac{\Delta_m}{\Delta_{um}} + \frac{E_{hm}}{V_y \Delta_{um}} \tag{18}$$

This defines a damage limit domain that relates the normalized plastic strain energy capacity of the component to the maximum [24]. The slope of the line is $-1/\beta^*$. The plastic strain energy E_h is estimated using the procedure given by Chai *et al.* [24]. The lack of sufficient experimental results on the substructures means that β^* cannot be evaluated for each component, and hence

monotonic and cyclic simulations of the 2D FE model by means of the IDARC 2D software [39] were performed. As a result, estimates of $E_h/V_y\Delta_{um}$ and Δ_m/Δ_{um} were defined for joint components with the corresponding best plots for each damage limit domain. The results are shown in Figure 12, and the highest value of β^* is related to the base joints and is $\beta^* = 0.21$. This clearly indicates the high capacity of the base joints in absorbing and dissipating cyclic energy through end plates and anchor yielding. The D_i values of joint components whose hysteretic behaviour is illustrated in Figure 10 are gathered in Table VIII. The values of D_i generally higher than 0.4, mirror both the design objectives and the severity of cyclic loads.
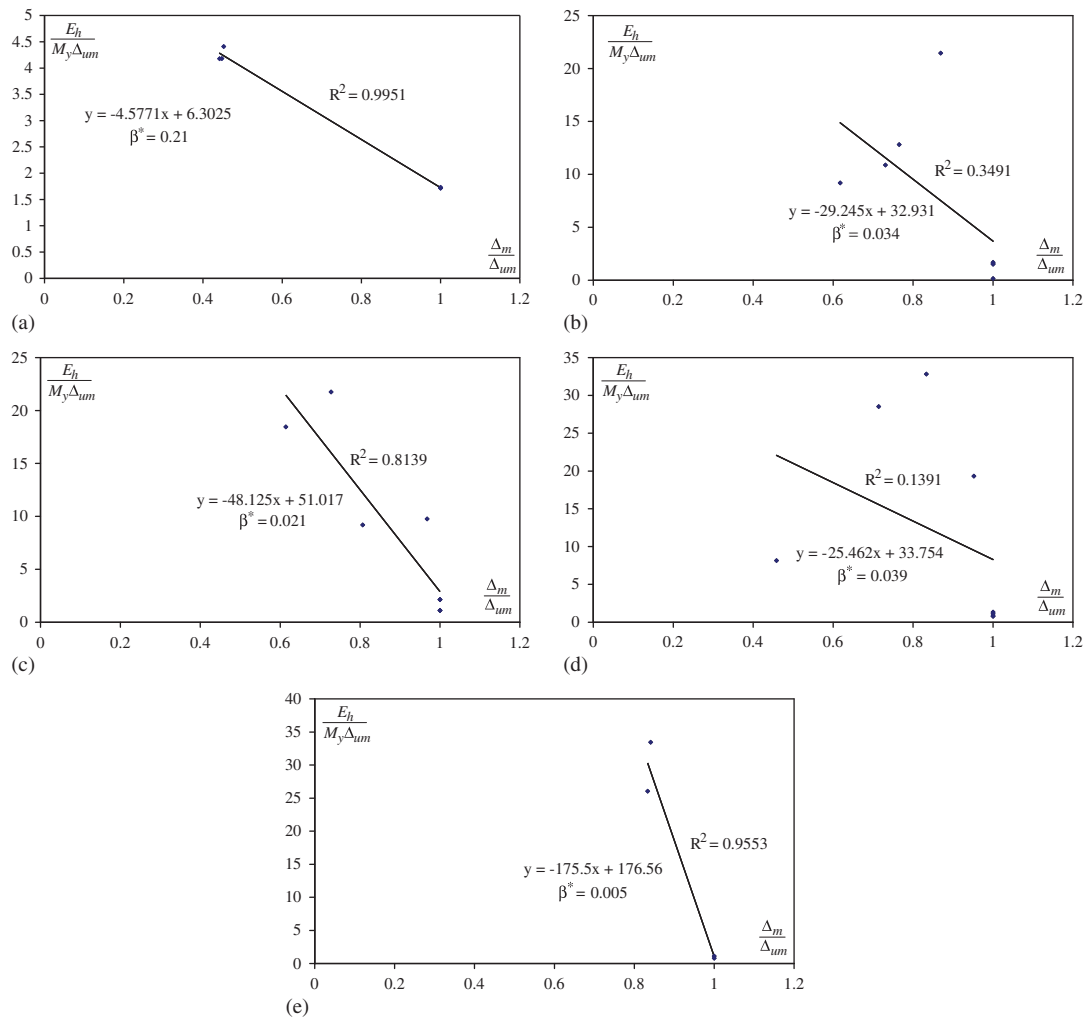

Figure 12. Damage limit domains and identified β^* parameter for joint components: (a) column base joints; (b) exterior connections; (c) interior connections; (d) exterior panels; and (e) interior panels.

Table VIII. Damage indices D_i of joint components using the model after Chai *et al.* [25].

Spring no.	3	4	6	7	8	15	16	17
D_i	0.34	0.90	0.89	0.96	0.78	0.55	0.63	0.48

Component numbers are taken from Figures 8 and 11.

6. CONCLUSIONS

The results summarized in this paper focused on the identification and damage estimation of a full-scale three-bay, two-storey steel–concrete composite MR structure with semi-rigid beam-to-column joints and partially encased composite columns. Forced vibration tests were performed at three different damage phases to detect the dynamic characteristics of the structure including stiffness degradation and strength deterioration.

A 3D finite element model of the structure was utilized and updated using the five lowest natural frequencies and related mode shapes. Beam-to-column joint stiffnesses were identified by using an innovative beam-to-column joint model able to take into account the deformability of both beam-to-column connections and web panels. The relevant cost function was minimized by a robust optimization algorithm, namely the Powell's Dog-Leg method, in order to update realistic stiffnesses of braces, columns, beam-to-column and column base joints. Moreover, experimental eigenvalues and eigenvectors and updated stiffnesses were employed to detect both the local and global damage of the structure, and these were consistent with the design objectives and visual inspection of the structure after each damage phase.

In order to assess the robustness of the identified parameters to measurement noise, a sensitivity analysis was carried out by means of the Latin Hypercube Sampling technique. This analysis indicated that in all damage phases the smallest coefficient of variation corresponded to the brace stiffnesses proving that braces were not so sensitive to input errors. Moreover, Phase III represented the least sensitive phase to measurement errors, because of the reliable initial parameters obtained from the cyclic model updating, and the flexibility of the structure owing to significant damage.

Only a small number of rotational components were retained during the modal updating exercise, because joint rotations were small in the lowest modes. This emphasizes the importance of the proper choice of location for accelerometers on members and joints of semi-rigid structures. In addition, a more sophisticated 3D FE model able to model floor flexibilities is required.

With regard to the final cyclic test, the acquisition of rotations, displacements and forces was exploited to update a 2D FE model of the structure by means of the Powell's Dog Leg optimization technique. A novel method based on the transformation of origin coordinates was implemented, in order to capture the hysteretic behaviour of joints. As a result, the internal actions of the structure were identified through updated parameters. Low-cycle fatigue joint damage was evaluated by means of an energy-based damage index and all estimates indicated irreparable damage. It was compatible both with the design objectives and with the severity of cyclic loadings.

REFERENCES

1. AISC. *ANSI/AISC 341-05. Seismic Provisions for Structural Steel Buildings.* American Institute of Steel Construction, Inc.: Chicago, IL, 2005.
2. CEN. Eurocode 8: design of structures for earthquake resistance. Part 1: general rules, seismic actions and rules for buildings. *EN 1998-1*, European Committee for Standardization, Brussels, Belgium, 2005.
3. Caramelli S, Salvatore W *et al.* Applicability of composite structure to sway frames. *ECSC Project n. 7210-PR-250*, *Eur Report*, European Community, 2004.
4. Bursi OS, Caramelli S, Fabbrocino G, Molina J, Taucer F, Salvatore W, Zandonini R. 3D full scale seismic testing of a steel-concrete composite building at ELSA. *Eur Report*, *EUR 21299 EN*, Joint Research Centre, European Community, Italy, 2004.
5. Braconi A, Bursi OS, Fabbrocino G, Salvatore W, Tremblay R. Seismic performance of a 3D full-scale high-ductility steel-concrete composite moment-resisting structure—part I: design and testing procedure. *Earthquake Engineering and Structural Dynamics* 2008; **37**(14):1609–1634. DOI: 10.1002/eqe.829.

6. Braconi A, Bursi OS, Fabbrocino G, Salvatore W, Taucer F, Tremblay R. Seismic performance of a 3D full-scale high-ductility steel-concrete composite moment-resisting structure—part II: test results and analytical validation. *Earthquake Engineering and Structural Dynamics* 2008; **37**(14):1635–1655. DOI: 10.1002/eqe.843.

7. Friswell MI, Mottershead JE. *Finite Element Model Updating in Structural Dynamics*. Kluwer Academic Publishers: Dordrecht, 1995.

8. Doebling SW, Farrar CR, Prime MB. A summary review of vibration-based damage identification methods. *The Shock and Vibration Digest* 1998; **30**(2):91–105.

9. Teughels A, Maeck J, De Roeck G. Damage assessment by FE modal updating using damage functions. *Computers and Structures* 2002; **80**(25):1869–1879. DOI: 10.1016/S0045-7949(02)00217-1.

10. Teughels A, De Roeck G. Structural damage identification of the highway bridge Z24 by FE model updating. *Journal of Sound and Vibration* 2004; **278**(3):589–610. DOI: 10.1016/j.jsv.2003.10.041.

11. Bakir PG, Reynders E, De Roeck G. An improved finite element model updating method by the global optimization technique 'Coupled Local Minimizers'. *Computers and Structures* 2008; **86**(11–12):1339–1352. DOI: 10.1016/j.compstruc.2007.08.009.

12. Rahai A, Bakhtiari-Nejad F, Esfandiari A. Damage assessment of structure using incomplete measured mode shapes. *Structural Control and Health Monitoring* 2007; **14**(5):808–829. DOI: 10.1002/stc.183.

13. Amani MG, Riera JD, Curadelli RO. Identification of changes in the stiffness and damping matrices of linear structures through ambient vibrations. *Structural Control and Health Monitoring* 2007; **14**(8):1155–1169. DOI: 10.1002/stc.206.

14. Sanayei M, Saletnik MJ. Parameter estimation of structures from static strain measurements. I: formulation. *Journal of Structural Engineering* 1996; **122**(5):555–562. DOI: 10.1061/(ASCE)0733-9445(1996)122:5(555).

15. Sanayei M, Saletnik MJ. Parameter estimation of structures from static strain measurements. II: errors sensitivity analysis. *Journal of Structural Engineering* 1996; **122**(5):563–572. DOI: 10.1061/(ASCE)0733-9445(1996)122:5(563).

16. Liu P-L, Chian C-C. Parametric identification of truss structures using static strains. *Journal of Structural Engineering* 1997; **123**(7):927–933. DOI: 10.1061/(ASCE)0733-9445(1997)123:7(927).

17. Wang X, Hu N, Fukunaga H, Yao ZH. Structural damage identification using static test data and changes in frequency. *Engineering Structures* 2001; **23**(6):610–621. DOI: 10.1016/S0141-0296(00)00086-9.

18. Wong CW, Mak WH, Ko JM. System and parametric identification of flexible connections in steel framed structures. *Engineering Structures* 1995; **17**(8):581–595. DOI: 10.1016/0141-0296(95)00010-5.

19. Koh CG, Qiao GQ, Quek ST. Damage identification of structural members: numerical and experimental studies. *Structural Health Monitoring* 2003; **2**(1):41–55. DOI: 10.1177/147592103031112.

20. Wu JR, Li QS. Structural parameter identification and damage detection for a steel structure using a two-stage finite element model updating method. *Journal of Constructional Steel Research* 2006; **62**(3):231–239. DOI: 10.1016/j.jcsr.2005.07.003.

21. Bursi OS, Molina J, Salvatore W, Taucer F. Dynamic characterization of a 3D full scale steel-concrete composite building at ELSA. *EUR21206EN*, Joint Research Centre, European Commission, Italy, 2004.

22. Petryna YS, Kratzig WB. Compliance-based structural damage measure and its sensitivity to uncertainties. *Computers and Structures* 2005; **83**(14):1113–1133. DOI: 10.1016/j.compstruc.2004.11.020.

23. McKay MD, Beckman RJ, Conover WJ. A comparison of three methods for selecting values of input variables in the analysis of output from a computer code. *Technometrics* 1979; **21**(2):239–245.

24. Chai YH, Romstad KM, Bird SM. Energy-based linear damage model for high-intensity seismic loading. *Journal of Structural Engineering* 1995; **121**(5):857–864. DOI: 10.1061/(ASCE)0733-9445(1995)121:5(857).

25. Salvatore W, Bursi OS, Lucchesi D. Design, testing and analysis of high ductile partial-strength steel–concrete composite beam-to-column joints. *Computers and Structures* 2005; **83**(28–30):2334–2352. DOI: 10.1016/j.compstruc.2005.03.028.

26. Ewins DJ. *Modal Testing*: *Theory*, *Practice and Application*. Research Studies Press Ltd: U.S.A., 2000.

27. Chellini G, De Roeck G, Nardini L, Salvatore W. Damage detection of a steel-concrete composite frame by a multilevel approach: experimental measurements and modal identification. *Earthquake Engineering and Structural Dynamics* 2008; **37**(15):1763–1783. DOI: 10.1002/eqe.835.

28. Madsen K, Nielsen HB, Tingleff O. Methods for non-linear least square problems. *Informatics and Mathematical Modelling*, Technical University of Denmark, 2004.

29. Wolfram Research, Inc. Mathematica, Version 6.0, Champaign, IL, 2007.

30. Jung H, Ewins DJ. Error sensitivity of the inverse eigensensitivity method for model updating. *10th International Modal Analysis Conference*, San Diego, CA, 3–7 February 1992; 992–998.

31. Fox RL, Kapoor MP. Rates of change of eigenvalues and eigenvectors. *AIAA Journal* 1968; **6**(12):2426–2429. DOI: 10.2514/3.5008.

32. Nelson RB. Simplified calculation of eigenvector derivatives. *AIAA Journal* 1976; **14**(9):1201–1205. DOI: 10.2514/3.7211.

33. Williams MS, Sexsmith RG. Seismic damage indices for concrete structures: a state-of-the-art review. *Earthquake Spectra* 1995; **11**(2):319–349. DOI: 10.1193/1.1585817.

34. Molinari M. Model updating of a steel-concrete composite MR frame structure under severe seismic loading via forced dynamic tests. *Ph.D. Thesis*, University of Trento, Italy, 2007.

35. McKay MD. Latin hypercube sampling as a tool in uncertainty analysis of computer models. *Winter Simulation Conference*, Arlington, VA, 13–16 December 1992; 557–564.

36. Iman RL, Conover WJ. A distribution-free approach to inducing rank correlation among input variables. *Communications in Statistics—Simulation and Computation* 1982; **11**(3):311–334. DOI: 10.1080/03610918208812265.

37. Ture Savadkoohi A. Inverse modelling of a steel-concrete composite moment resisting structure subjected to severe cyclic loads and forced vibration tests. *Ph.D. Thesis*, University of Trento, Italy, 2008.

38. S-PLUS® (version6.1). Insightful Corporation, Seattle, WA, 2001.

39. IDARC2D. *A Computer Program for Seismic Inelastic Structural Analysis*, *Version 5.5*, Department of Civil, Structural and Environment Engineering, University of Buffalo, U.S.A., 2002.